THE JOURNAL OF PHYSICAL CHEMISTRY B

Article

pubs.acs.org/JPCB

ESEEM Analysis of Multi-Histidine Cu(II)-Coordination in Model Complexes, Peptides, and Amyloid-β

K. Ishara Silva, Brian C. Michael, Steven J. Geib, and Sunil Saxena*

Department of Chemistry, University of Pittsburgh, Pittsburgh, Pennsylvania 15260, United States

Supporting Information

ABSTRACT: We validate the use of ESEEM to predict the number of ^{14}N nuclei coupled to a Cu(II) ion by the use of model complexes and two small peptides with well-known Cu(II) coordination. We apply this method to gain new insight into less explored aspects of Cu(II) coordination in amyloid-β (Aβ). Aβ has two coordination modes of Cu(II) at physiological pH. A controversy has existed regarding the number of histidine residues coordinated to the Cu(II) ion in component II, which is dominant at high pH (~8.7) values. Importantly, with an excess amount of Zn(II) ions, as is the case in brain tissues affected by Alzheimer's disease, component II becomes the dominant coordination mode, as Zn(II) selectively substitutes component I bound to Cu(II). We confirm that component II only contains single histidine coordination, using ESEEM and set of model complexes. The ESEEM experiments carried out on systematically ^{15}N-labeled peptides reveal that, in component II, His 13 and His 14 are more favored as equatorial ligands compared to His 6. Revealing molecular level details of subcomponents in metal ion coordination is critical in understanding the role of metal ions in Alzheimer's disease etiology.

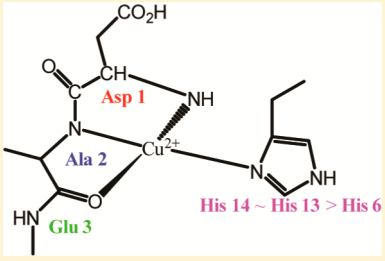

INTRODUCTION

Among natural amino acids histidine is one of the strongest metal ion coordinators.[1] Hence, histidine plays an important role in metal ion coordination in proteins and peptides. Histidine is a tridentate ligand, which provides ligands at the imidazole imido nitrogen, the amino nitrogen, and the carboxylate oxygen.[2] The imidazole ring nitrogen of histidine residues often provides the primary coordination site for metal ions.[2] Copper is an essential metal ion for biological functions and is found in bound forms in metalloproteins and in low molecular weight complexes to avoid toxicity associated with free copper.[2] Copper-containing proteins often have binding sites with irregular geometries containing one or more histidine ligands.

Copper coordination in amyloidogenic proteins such as amyloid-β (Aβ), prion, and α-synuclein is achieved through histidine residues.[3] All these systems contain highly heterogeneous copper coordination environments. Small changes in the coordination may have an effect on aggregation and other chemical mechanisms in the diseased state.[4] Hence, it is critical to elucidate the structural details of the different coordination modes to completely understand the biological role played by metal−protein complexes.[1]

In α-synuclein two Cu(II) coordination sites at the N-terminal region were identified using mass spectrometry (MS)[5] and nuclear magnetic resonance (NMR).[6] Later circular dichroism (CD)[6] and electron spin resonance (ESR) results indicated that these sites are independent of each other.[7−9] The high affinity site is anchored by the N-terminus, and the second site is anchored by the histidine at position 50.[10] Other than these two sites, recent NMR and ESR results propose a low affinity Cu(II) binding site at the C-terminal region.[7,11] In prion protein the presence of four binding sites at higher Cu(II) occupancy in each of the PHGGGWGQ octarepeat regions were identified based on ESR,[12−17] CD,[12−14] NMR,[18,19] and X-ray absorption spectroscopy (XAS)[20,21] results. Two additional Cu(II) equivalents coordinate via the histidine residues located at positions 96 and 111.[3,15,16,20] Additionally, the Cu(II) coordination environment in prion octarepeat domain has been extensively studied by ab initio methods.[22−24]

The copper coordination to Aβ is highly heterogeneous, with the specific coordination environment depending on the pH, ionic strength, concentration of the metal ions, and the presence of other metal ions. The metal binding domain of Aβ contains three histidine residues at positions 6, 13, and 14.[4,25] The presence of all three histidine residues in Cu(II) coordination spheres was initially proposed by NMR[25,26] and was later confirmed by ESR.[27] Other techniques such as XAS,[28,29] Fourier transform infrared spectroscopy (FTIR),[4,30] CD,[25,31,32] ultraviolet−visible (UV−vis),[32] MS,[33] and ab initio calculations[28,34,35] also proposed the involvement of histidine residues in Cu(II) coordination. A number of ESR studies have suggested an equilibrium between two different Cu(II) coordination modes in an equimolar Aβ−Cu(II) complex at pH 7.4, known as component I and component II.[25,36−41] The component I is predominant at lower pH values (~pH 6.0).[4] Component II is dominant at higher pH (~pH 8.7).[4] These two components are believed to have a different number of histidine residues coordinated to the Cu(II) ion.[42] Component I is believed to have two histidine residues that simultaneously

Received: January 22, 2014
Revised: July 10, 2014
Published: July 11, 2014

   dx.doi.org/10.1021/jp500767n | J. Phys. Chem. B 2014, 118, 8935−8944

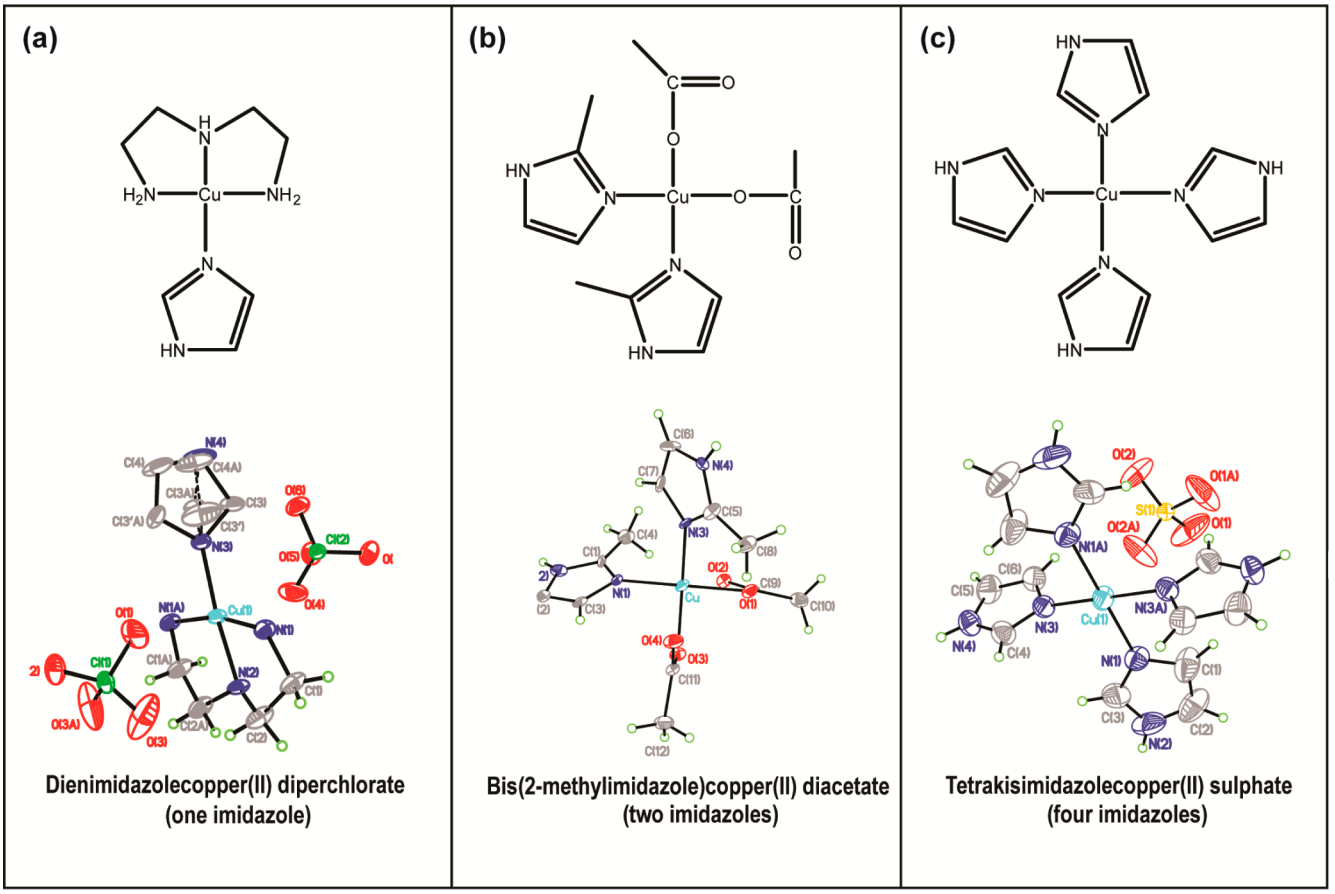

Figure 1. Structures of the model complexes with 1, 2, and 4 imidazole rings and their crystal structures.

coordinate to Cu(II).[38,42] Previously we used electron spin echo envelope modulation (ESEEM) in conjunction with ^{15}N isotopic labeling, to determine that the Aβ component I consists of three subcomponents, at physiological pH where two of the three histidines are simultaneously coordinated to Cu(II) ion.[38] Interestingly, only two of these subcomponents, are present at lower pH values.[42,43] Cu(II) coordinated to His 6−His 13 and His 6−His 14 are found in equal proportions, while the His 13−His 14 coordination is absent at lower pH.[38,43] These measurements were able to uncover the critical role of His 13−His 14 in Cu(II) coordination at physiological pH and provide a possible rationale for the presence of amorphous aggregates, rather than fibrils at high Cu(II) concentrations.[38,44]

The number of histidine residues coordinated to Cu(II) in component II is controversial. One hypothesis proposes that Cu(II) is coordinated to the CO group of the Ala 2−Glu 3 bond and three histidine residues.[40] The second proposition involves the N-terminus, one N atom from one of the three histidine imidazoles, the backbone N from Asp 1-Ala 2 peptide bond, and the CO group of the Ala 2−Glu 3 peptide bond.[43] The coordination of Cu(II) in component II is believed to be highly dynamic. The elucidation of the coordination in component II is critical as a recent research shows that, in the presence of Zn(II), Cu(II) coordination moves to a component II-like coordination.[39,45] Furthermore, it has been shown that Zn(II) can only displace Cu(II) from component I coordination.[39] One equivalent of Zn(II) ions displaces ∼25% of the bound Cu(II) from Aβ(1−16) at physiological pH, while rearranging the rest of the bound Cu(II) in component I.[39] In the presence of one equivalent of Zn(II) ions, components I and II account equally for Cu(II) coordination in Aβ.[39] However, at excess amounts of Zn(II), component II becomes the dominant Cu(II) coordination mode.[39] In brain tissues affected by the Alzheimer's disease, the concentration of Zn(II) is approximately three times higher than Cu(II).[46] Therefore, component II Cu(II) coordination may be the most dominant coordination mode in vivo. Shedding light into the coordination of component II is critical to understand the behavior of Cu(II) in AD etiology.

Herein, we propose a method to quantify the number of ^{14}N nuclei coordinated to a Cu(II) center by the use of integrated intensities of the Fourier-transformed ESEEM. ESEEM spectroscopy is a pulsed ESR technique that has been used to identify and quantify the number of histidine imidazoles coupled to a Cu(II) center. Spectral simulations of the ESEEM spectra are used to determine the number of coupled ^{14}N nuclei.[47,48] Alternatively, Shin et al. compared the normalized integrated intensities of the frequency domain ESEEM spectra to calculate the intensity reduction resulting from the replacement of a ^{14}N with ^{15}N in Aβ(1−16)−Cu(II) complexes.[38] Although, the use of integration method was useful in elucidating important structural information, the validity of the method was not tested experimentally. Here we obtained ESEEM data from simple model complexes with different numbers of imidazoles coordinated to Cu(II). The normalized integrated intensities of the model complexes increased monotonically, when the number of imidazole rings increased in model complexes. Two small peptides with known Cu(II) coordination was used to test the validity of the method.

dx.doi.org/10.1021/jp500767n | J. Phys. Chem. B 2014, 118, 8935−8944

The DAHK−Cu(II) complex contains a single ^{14}N ESEEM active nucleus, while PHGGGW−Cu(II) complex contains two nonidentical ^{14}N ESEEM active nuclei. Finally, our method was used to distinguish between the two proposed modes of Cu(II) coordination. Then, in conjunction with ^{15}N isotopic labeling we quantified the subcomponent proportions in component II.

EXPERIMENTAL SECTION

Synthesis of Copper−Imidazole Complexes. For the preparation of tetrakisimidazolecopper(II) sulfate (see Figure 1a), 40 mL of a 1 M imidazole (99% Sigma-Aldrich Co., St. Louis, MO) solution was added to 10 mL of 1 M $CuSO_4 \cdot 5H_2O$ (98+% Sigma-Aldrich Co., St. Louis, MO) solution and left at room temperature to evaporate. After a few days, dark blue colored crystals formed.[49] For the preparation of bis(2-methylimidazole)copper(II) diacetate[50] (see Figure 1b), 0.5 g of Cu(II) acetate hydrate (98% Sigma-Aldrich Co., St. Louis, MO) and 1.0 g of 2-methylimidazole (99% Sigma-Aldrich Co., St. Louis, MO) were added and dissolved in a mixture of chloroform (10 mL) and methanol (2.5 mL). This mixture was stirred for 30 min at 50 °C and filtered. Then, 15 mL of diethyl ether was added to the filtrate and stirred for 10 min. Then another 5 mL of diethyl ether was added and filtered under reduced pressure and washed with diethyl ether and chloroform. The solid was air-dried and recrystallized from methanol/diethyl ether. For dienimidazolecopper(II) diperchlorate (see Figure 1c), 30 mL of 2 mM $Cu(ClO_4)_2 \cdot 6H_2O$ (98% ACROS Organics, New Jersey) in a methanol/acetonitrile (5:1) mixture was stirred with 3 mL of 2 mM triethylenediamine (≥97% Fluka, Netherlands) in water. Then, 10 mL of 2 mM imidazole in methanol was added to the mixture. After being left overnight, blue colored crystals were obtained.[51] All the solvents used in synthesis were purchased from Sigma-Aldrich Co., St. Louis, MO. Crystals were dissolved in water to make 10 mM stock solutions. For ESR experiments, samples were prepared in the presence of 25% (v/v) glycerol (≥99% Sigma-Aldrich Co., St. Louis, MO), with a final Cu(II) concentration of 1.25 mM.

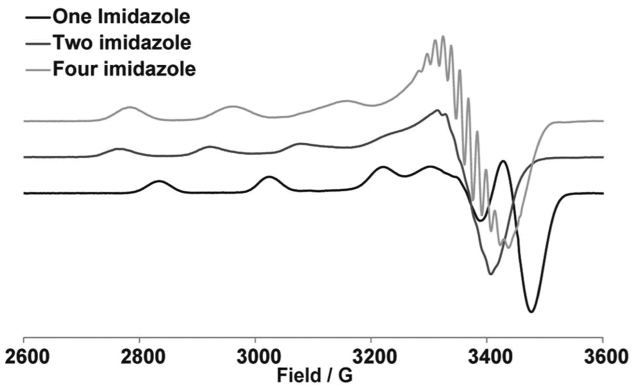

Figure 2. CW-ESR spectra of model complexes.

The peptide PHGGGW, the Cu(II) binding domain of prion, was synthesized at the Molecular Medicine Institute, University of Pittsburgh, using standard fluorenylmethoxycarbonyl chemistry.[52,53] Isotopically enriched [G-^{15}N]-N_α-Fmoc-N_τ-trityl-L-histidine was purchased from Cambridge Isotope Laboratory (Andover, MA), in which all nitrogen atoms are ^{15}N enriched. Three different variants of amyloid-β(1−16) (DAEFRHDSGYEVHHQK) with each containing an ^{15}N enriched histidine at either position 6, 13, or 14 were synthesized at the Molecular Medicine Institute, University of Pittsburgh, using standard fluorenylmethoxycarbonyl chemistry.[52,53] Double-labeled peptides containing two ^{15}N enriched histidine residues were synthesized in the same manner. All the labeled amyloid-β (1−16) variants were purified by high-performance liquid chromatography and characterized by mass spectroscopy. Nonlabeled amyloid-β (1−16) peptide was purchased from rPeptide (Bogart, GA). The peptide fragment DAHK, the N-terminus region of the human serum albumin, was purchased from Fisher Scientific, Hanover Park, IL. Amyloid-β (1−16) peptide was purchased from rPeptide (Bograt, GA). For peptide samples, the concentration of the peptide was 1.25 mM and an equimolar amount of Cu(II) was present in both the samples. Samples were prepared in *N*-ethylmorpholine (NEM) buffer at pH 7.4 in 25% (v/v) glycerol and appropriate amounts of hydrochloric acid.

Single Crystal X-ray Data Collection. X-ray diffraction data for the one-imidazole and two-imidazole model complex structures were collected using a single crystal on a Bruker X8 Prospector Ultra CCD diffractometer with a CuKα (λ = 1.54178 A) ImuS radiation source. The parameters used during the collection of diffraction data for each structure are summarized in Supporting Information. Crystals were mounted in Fluorolube oil on a Mitegen mount and placed in a cold N_2 stream (150(1) K) for data collection. X-ray diffraction data for the four-imidazole model complex was collected on a Bruker Smart Apex CCD diffractometer with graphite-monochromated MoKα (λ = 0.71073 Å) radiation at room temperature. A single crystal was mounted with epoxy onto a glass fiber.

For each structure, unit-cell dimensions were derived from the least-squares fit of the angular settings of 999 strong reflections from the data collection. Data were corrected for absorption using the Bruker AXS program SADABS. Each structure was solved via direct methods, which located the positions of the non-hydrogen atoms. All non-hydrogen atoms were refined anisotropically. Final difference Fourier syntheses showed only chemically insignificant electron density. An inspection of F_o vs F_c values and trends based upon sin θ, Miller index, or parity group failed to reveal any systematic error in the data. All computer programs used in the data collection and refinements are contained in the Bruker program package Apex2 v.2013.10−0.

All three crystal structures have been reported previously, and our results are in substantial agreement with those previously reported structures.[49−51]

Electron Spin Resonance Spectroscopy. A 200 μL aliquot of complex samples with a concentration of 1.25 mM was transferred into a quartz tube with an inner diameter of 3 mm. Glycerol (25%, v/v) was added as a cryoprotectant. All ESR experiments were performed on a Bruker ElexSys E580 X-band or a Bruker ElexSys E680 X-band FT/CW spectrometer equipped with Bruker ER4118X-MD5 and EN4118X-MD4 resonators, respectively. The temperature was controlled using an Oxford ITC503 temperature controller and an Oxford CF935 dynamic continuous flow cryostat connected to an Oxford LLT 650 low-loss transfer tube. Continuous-wave ESR experiments were carried out on sample solutions at 80 K and at X-band microwave frequency. The magnetic field was swept from 2600 to 3600 G for 1024 data points. A time constant of 10.24 ms, a conversion time of 20.48 ms, modulation amplitude of 4 G, a modulation frequency of 100 kHz, and a microwave

dx.doi.org/10.1021/jp500767n | J. Phys. Chem. B 2014, 118, 8935−8944

power of 0.1993 mW were the other instrument parameters used for the CW experiment.

The three-pulse ESEEM experiments were performed on the sample solutions at 20 or 80 K, by using a $\pi/2 - \tau - \pi/2 - T - \pi/2$-echo pulse sequence with a $\pi/2$ pulse width of 16 ns. The first pulse separation, τ, was set at 144 ns, and the second pulse separation, T, was varied from 288 ns with a step size of 16 ns. The experiments were carried out at the magnetic field, where the ESR intensity was maximum. A four-step phase cycling was employed to eliminate unwanted echoes.[54,55] The raw data was phase corrected, and the real part was selected. After the baseline correction, the spectra were fast Fourier-transformed. Then the final spectra were obtained as the magnitude of the Fourier transforms.

ESEEM Data Analysis. We normalized the ESEEM spectra using the integrated intensity of ^{1}H ESEEM signal (13−16 MHz). Possible limitations of the above method are discussed in the results section.

For a single ^{14}N nucleus coupled to an electron spin, the relative modulation depth is[38]

$$K_{14}^{\alpha}/K_1 = \frac{K_{14}^{\alpha}(1 - K_1)}{K_1(2 - K_{14}^{\alpha} - K_{14}^{\beta})} \tag{1}$$

where K is the modulation depth and subscripts 14 and 1 denote the ^{14}N and ^{1}H spin, respectively. Superscripts α and β denote the α and β spin manifolds of the electron spin, respectively.[38]

For two equivalent ^{14}N nuclei coupled to an electron spin the relative modulation depth becomes[38]

$$K_{14}^{\alpha'}/K_1 = \frac{4K_{14}^{\alpha}(1 - K_{14}^{\alpha})(1 - K_1)}{K_1[2(1 - K_{14}^{\alpha})^2 + (K_{14}^{\alpha})^2 + 2(1 - K_{14}^{\beta})^2 + (K_{14}^{\beta})^2]} \tag{2}$$

$K_{14}^{\alpha\prime}$ is the modulation depth of the α spin manifolds of the two equivalent ^{14}N nuclei. The relative modulation depth of ^{14}N increases with the addition of the ^{14}N nucleus, and the factor of increase is given by

$$\frac{(K_{14}^{\alpha'}/K_1)}{(K_{14}^{\alpha}/K_1)} = \frac{4(1 - K_{14}^{\alpha})(2 - K_{14}^{\alpha} - K_{14}^{\beta})}{2(1 - K_{14}^{\alpha})^2 + (K_{14}^{\alpha})^2 + 2(1 - K_{14}^{\beta})^2 + (K_{14}^{\beta})^2} \tag{3}$$

If K_{14}^{α} and K_{14}^{β} are much smaller than 1, the factor converges to 2. The theoretical value for K_{14}^{α} and K_{14}^{β} is approximately 0.15, for a $\pi/2$ pulse length of 16 ns.

If two nonequivalent ^{14}N nuclei are coupled to the electron spin, the relative modulation depth is given as[38]

$$K_{14}^{\alpha''}/K_1 = \frac{(K_{14}^{\alpha} + K_{14'}^{\alpha} - 2K_{14}^{\alpha}K_{14'}^{\alpha})(1 - K_1)}{K_1[(1 - K_{14}^{\alpha})(1 - K_{14'}^{\alpha}) + (1 - K_{14}^{\beta})(1 - K_{14'}^{\beta})]} \tag{4}$$

$K_{14}^{\alpha\prime\prime}$ is the modulation depth of the α spin manifolds of the two nonequivalent ^{14}N nuclei. The increase in the relative modulation depth with the additional ^{14}N nuclei is given by

$$\frac{(K_{14}^{\alpha''}/K_1)}{(K_{14}^{\alpha}/K_1)} = \frac{(K_{14}^{\alpha} + K_{14'}^{\alpha} - 2K_{14}^{\alpha}K_{14'}^{\alpha})(2 - K_{14}^{\alpha} - K_{14}^{\beta})}{K_{14}^{\alpha}[(1 - K_{14}^{\alpha})(1 - K_{14'}^{\alpha}) + (1 - K_{14}^{\beta})(1 - K_{14'}^{\beta})]} \tag{5}$$

If K_{14}^{α}, $K_{14'}^{\alpha}$, K_{14}^{β}, and $K_{14'}^{\beta}$ are much smaller than 1, eq 5 simplifies to

$$\frac{(K_{14}^{\alpha''}/K_1)}{(K_{14}^{\alpha}/K_1)} = 1 + \frac{K_{14'}^{\alpha}}{K_{14}^{\alpha}} \tag{6}$$

If two ^{14}N nuclei are equivalent (i.e., $K_{14}^{\alpha} = K_{14'}^{\alpha}$), the factor in eq 6 becomes 2.

However, obtaining modulation depth information from ESEEM time domain data is difficult as many components are overlaid in the signal. It has been shown that integrated intensities can be used to account for the changes in the modulation depth.[38] In the frequency domain ^{14}N ESEEM signal is well separated from the ^{1}H ESEEM signal, so it is possible to integrate separately. The ^{14}N ESEEM intensity is obtained by integrating between 0−11 MHz, and the ^{1}H ESEEM intensity is obtained for the region between 13−16 MHz.

RESULTS AND DISCUSSION

In this work we experimentally determine the validity of the use of ESEEM integration intensities to quantify the number of ^{14}N nuclei coupled to a Cu(II) center. To this end a series of model complexes with different numbers of imidazole ligands coordinated to copper are used. Then, the ESEEM analysis was carried out on two small peptides with known Cu(II)−histidine coordination, namely DAHK and PHGGGW peptides. The DAHK peptide is the N-terminus region of the human serum albumin (HSA) and coordinate Cu(II) in the well characterized ATCUN motive.[56] The DAHK−Cu(II) complex contains a single ^{14}N ESEEM active nucleus through the histidine imidazole coordination. The peptide PHGGGW is a truncated fragment of the octarepeat Cu(II) binding domain of the prion protein and has a known Cu(II) coordination including a crystal structure.[57] The PHGGGW−Cu(II) complex is specifically used as there are two nonidentical ^{14}N ESEEM active nuclei coupled to Cu(II). One ^{14}N nucleus is from the histidine imidazole coordination and the other from the peptide backbone coordination.[15] Then we used ESEEM to distinguish between the two proposed modes of coordination for component II of Aβ. Furthermore, the proportions of each histidine residue coordinated to Cu(II) ion as an equatorial ligand were measured with the use of systematic ^{15}N-labeled histidine residues.

Electron Spin Resonance of Model Complexes. In copper−imidazole complexes, the imidazole ring has a noncoordinated distal nitrogen, which contributes toward the ESEEM signal at X-band frequencies (~9.5 GHz), with pulse lengths used in this work ($\pi/2$ = 16 ns).[58] Hence, the ^{14}N ESEEM intensity will increase with the addition of imidazole rings to the coordination. In order to quantify the increase in ^{14}N ESEEM intensity we synthesized three model complexes (shown in Figure 1) containing 1, 2, and 4 imidazoles coordinated to a copper center, respectively. All three complexes were synthesized as crystals, and the structure of the complexes was verified using X-ray crystallography. The

dx.doi.org/10.1021/jp500767n | J. Phys. Chem. B 2014, 118, 8935−8944

crystal structures of the complexes are shown in Figure 1. All these structures contain copper centers coordinated with four equatorial ligands according to the information gained from crystal structures. In the one-imidazole and the four-imidazole complexes, structures of the counterion ligands perchlorate and the sulfate, respectively, are resolved as shown in Figure 1. ESR measurements are less sensitive to axial ligands[31] and are not considered in the analysis. The one-imidazole complex contains four directly coordinated nitrogens; three from the tridentate ligand, and one from the imidazole ring. Directly coordinated nitrogens do not contribute to ESEEM at X-band, with pulse lengths used in this work. The one-imidazole model complex contains just single ^{14}N ESEEM active nuclei, which is in the imidazole ring.

First, CW-ESR experiments were carried out on the model complexes. As shown in Figure 2, the one-imidazole complex has $g_{\|}$ and $A_{\|}$ values of (2.22 ± 0.005) and (191 ± 1) Gauss, respectively. These ESR parameters correspond to four nitrogen nuclei coordinated to the Cu(II) center in the equatorial plane,[59] which is consistent with the structure of the one-imidazole complex, as shown in Figure 1a. The two-imidazole complex has $g_{\|}$ and $A_{\|}$ values of (2.30 ± 0.005) and (158 ± 1) Gauss, respectively, which is consistent with a two nitrogen and two oxygen nuclei equatorial coordination.[59] For the four-imidazole complex, $g_{\|}$ and $A_{\|}$ values are (2.26 ± 0.005) and (182 ± 1) Gauss, respectively, which again is consistent for four directly coordinated nitrogen nuclei.[59] Hence, CW-ESR parameters clearly show that model complexes maintain the same Cu(II) coordination environment in solution.

Then the ESEEM experiments were performed on model complexes. The ESEEM spectra of these complexes are shown in Figure 3. Nuclear quadrupole interactions (NQI) of ^{14}N give

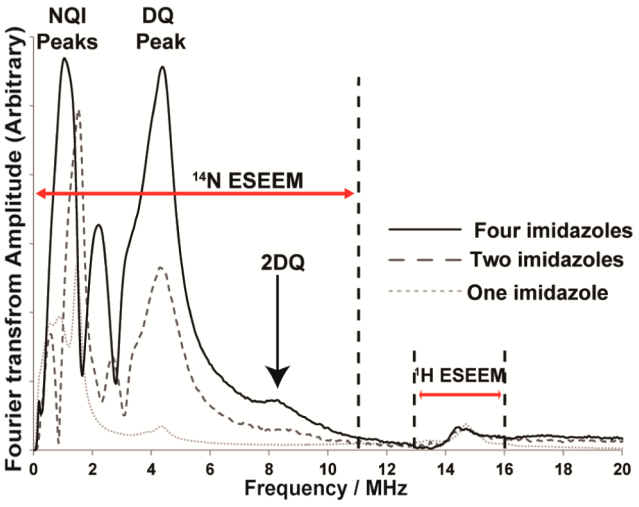

Figure 3. Experimentally obtained three-pulse ESEEM spectra of the model complexes at the maximum $g_{\perp}$ position. Appearance of a peak around 9 MHz in two- and four-imidazole complexes is indicative of multiple imidazole coordination.

rise to features below 2 MHz. The broad feature around 4 MHz is due to the double quantum (DQ) transition of the remote nitrogen in an imidazole ring.[57,58] The intensity of the DQ peak increases with the number of imidazole rings coordinated to the Cu(II) center.[48] A peak around 9 MHz (black arrow in Figure 3) is also indicative of multiple imidazole coordination.[48,60] This peak is clearly observed in the two- and four-imidazole complexes.

The integrated intensity for ^{14}N-ESEEM was calculated for the region between 0−11 MHz and then divided by the ^{1}H-ESEEM intensity integrated between 13 and 16 MHz. Details of the error calculation are provided in the Supporting Information (see Figure S3). The normalized ^{14}N-ESEEM intensity increases from 8.4 to 21 when going from single imidazole to two imidazoles as shown in Table 1. When there

Table 1. Integrated Intensities of the Peaks at the ^{14}N-ESEEM Region (0−11 MHz) and ^{1}H-ESEEM Region (13−16 MHz) and the Ratio of ^{14}N to ^{1}H Integrated Intensities[a]

complex	^{14}N-ESEEM	^{1}H-ESEEM	^{14}N/^{1}H
four-imidazole	3486 ± 3	87 ± 2	40 ± 1.5
two-imidazole	1868 ± 2	87 ± 1	21 ± 1.0
one-imidazole	723 ± 0.4	86 ± 0.2	8.4 ± 0.1
DAHK	603 ± 0.4	86 ± 0.2	7.0 ± 0.1
PHGGGW	1875 ± 0.7	86 ± 0.2	22 ± 0.1
Aβ(1−16) pH 8.7	1412 ± 0.7	87 ± 0.2	17 ± 0.1

[a]In the text, values in the last column are referred as normalized integrated intensity.

are four imidazoles coordinated to the Cu(II) center, normalized ^{14}N-ESEEM intensity is increased to 40. Hence, there is a monotonic increase in the normalized ^{14}N-ESEEM intensity with the increase of number of imidazole rings coordinated.

ESEEM Analysis on Cu(II)−Peptide Complexes with Known Coordination. In order to test our claim in a biologically relevant system, ESEEM experiments were conducted on two different peptide fragments with well-known Cu(II) coordination. The four amino acid peptide DAHK is the N-terminus fragment of the human serum albumin.[56] In the DAHK peptide, the imidazole ring of the histidine residue coordinates to the Cu(II) ion, and the distal nitrogen of the imidazole ring is the only ESEEM active nuclei as shown in Figure 4. The comparison between the ESEEM spectra of Cu(II)−DAHK and one-imidazole complex is shown in Figure 4. Both complexes show the characteristic three NQI peaks and the broad DQ peak. The intensities of the DQ peaks

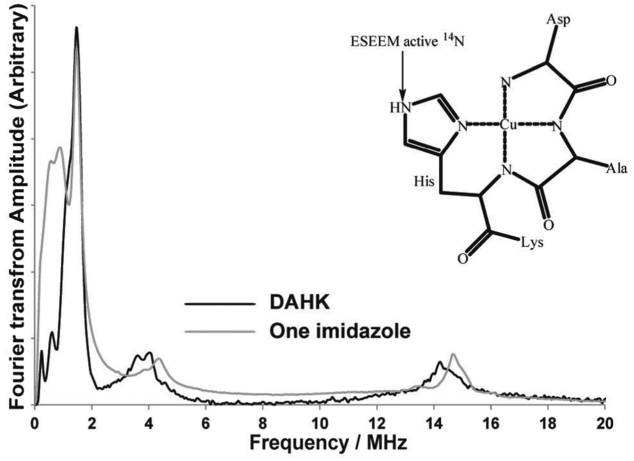

Figure 4. Comparison of ESEEM spectra of Cu(II)−DAHK complex and one-imidazole complex. Only one ^{14}N-ESEEM active nuclei is present in the reported coordination of DAHK.

dx.doi.org/10.1021/jp500767n | J. Phys. Chem. B 2014, 118, 8935−8944

are comparable in the two complexes. The intensity of DQ peak reflects the number of imidazoles coordinated to the Cu(II) center.[61] The normalized integrated intensity for Cu(II)−DAHK is 7.0 ± 0.1 compared to 8.4 ± 0.1 for the one-imidazole complex (Table 1).

Then we used the PHGGGW peptide fragment, which is the Cu(II) binding domain of the prion protein.[17,57] Burns et al. resolved the Cu(II) coordination environment of the octarepeat fragment using ESR experiments and a crystal structure of the Cu(II)−PHGGGW complex.[57] As shown in Figure 5, Cu(II) is coordinated to an imidazole nitrogen in a

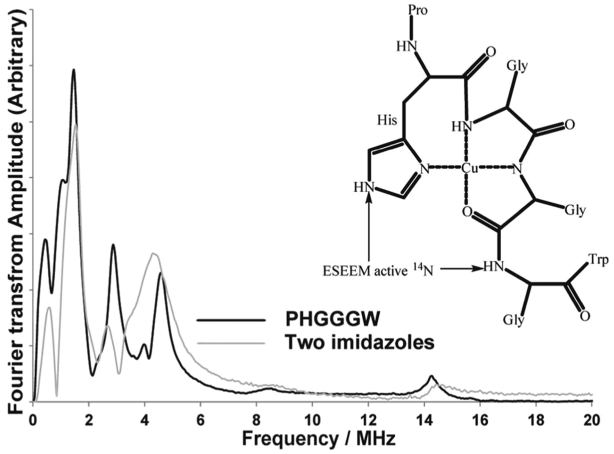

Figure 5. Comparison of ESEEM spectra of Cu(II)−PHGGGW complex and the two-imidazole complex. Cu(II)−PHGGGW complex contains two ^{14}N-ESEEM active nuclei.

histidine, two backbone nitrogens from two glycine residues, and an oxygen from a carboxylic group. The structure of the Cu(II) bound HGGGW pentapeptide was found to be unstable in solution due to the breaking of the axial water coordination.[22] However, the complex still maintains the equatorial square planar coordination.[22] Also, ESEEM results have indicated that histidine imidazole coordination and backbone coordination is present in the Cu(II)−PHGGGW complex in solution.[12,15] The ESEEM spectra of the Cu(II)−PHGGGW complex and the two-imidazole complex are shown in Figure 5 for comparison. Given the different coordination environments the two spectra do not have identical peak positions. Importantly, the intensity of the DQ peak is different. The two-imidazole complex has a larger DQ peak compared to the PHGGGW complex. The reported structure for the Cu(II)−PHGGGW structure contains two ^{14}N-ESEEM active nuclei from the distal nitrogen of the imidazole histidine and the backbone coordination as shown in Figure 5.[15] Hence, the intensity of DQ peak is expected to be different between the two complexes, as DQ peak intensity is indicative of the number of imidazoles coordinated.[47,61] However, the normalized ^{14}N-ESEEM integrated intensity obtained for the Cu(II)−PHGGGW complex is similar to the integrated intensity of the two-imidazole complex. This information verifies that the integration method can predict the number of ^{14}N nuclei coupled to a Cu(II) center.

Quantification of Histidine Residues Coordinated to Component II of Cu(II)−Aβ(1−16) Complex. The integration analysis was used to determine the number of nitrogens coupled to the Cu(II) ion in Aβ(1−16) in component II. As shown in the inset of Figure 6, Zn(II) selectively displaces

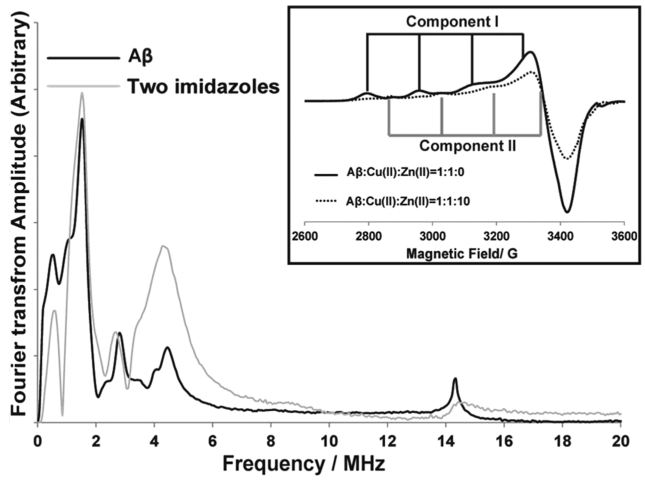

Figure 6. Comparison of ESEEM spectra of Cu(II)−Aβ(1−16) complex at pH 8.7 and the two-imidazole complex. The inset shows the increase of component II Cu(II) contribution in the presence of Zn(II).

Cu(II) coordinated to component I. At excess amounts of Zn(II) (ten equivalents of Zn(II)), component II accounts for ∼65% of the overall coordination (inset of Figure 6), where in the absence of Zn(II) the percentage is only 35%.[39] Amyloid aggregates in brain tissues contain approximately three times Zn(II) than Cu(II).[46] Hence, component II becomes the dominant Cu(II) coordination mode in vivo. Figure 6 shows the comparison between the two-imidazole complex and the Aβ(1−16)−Cu(II) complex at pH 8.7. At pH 8.7 only the component II of Cu(II) coordination exists.[4,43] The integrated intensities tabulated in Table 1 suggest that two ^{14}N nucleus are coupled to the Cu(II) ion. The features of the ESEEM spectrum clearly illustrate the imidazole histidine coordination as shown in Figure 6. The peak around 2.8 MHz is indicative of backbone coordination.[57] The backbone coordination peak is possibly due to the coupling between the Cu(II) ion with the remote backbone nitrogen nuclei of Glu 3, where Cu(II) is coordinated to the carbonyl oxygen of Ala 2.[40] This suggests just a single histidine residue is coordinated to Cu(II) in component II coordination.

The normalized integrated intensity (^{14}N-ESEEM/^{1}H-ESEEM) of Aβ(1−16) is 17 compared to 21 and 22 for the two-imidazole complex and the PHGGGW, respectively. The lower value for Aβ(1−16) is possibly due to the smaller number of protons that interact with the Cu(II) center. The Cu(II) centers in the model complexes are solvent accessible. In Aβ(1−16) the solvent−Cu(II) interaction may be restricted because of the neighboring amino acids. In our analysis we have normalized the integrated area of the ^{1}H-ESEEM peak to be the same for all spectra. Therefore, we may be underestimating the ^{14}N-ESEEM integrated intensity for Aβ(1−16). Nevertheless, the normalization method does suggest that Cu(II) is coupled to two ^{14}N-ESEEM active nuclei, not one or three. Hence, we can answer the crucial question of the number of histidines coordinated to component II.

Contributions of Each Histidine toward Component II and Physiological Importance. Three-pulse ESEEM spectroscopy was used in conjunction with isotopic substitution to determine the coordination of component II. Specifically the aim of these experiments was to provide more insight into the proportions of histidine residues involved in component II

dx.doi.org/10.1021/jp500767n | J. Phys. Chem. B 2014, 118, 8935−8944

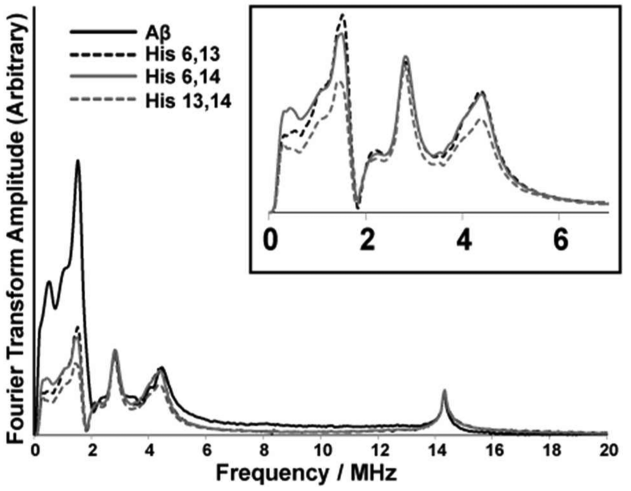

Figure 7. Three-pulse ESEEM spectra of the nonlabeled and single ^{15}N-labeled Aβ(1−16) variants mixed with equimolar amounts of Cu(II) at pH 8.7. The decrease in intensity below 8 MHz in ^{15}N-labeled Aβ(1−16) variants gives the contribution of each histidine residue for component I in Aβ(1−16)−Cu(II). The inset shows an expanded view of the 0−6 MHz region for the labeled peptides.

coordination. First, double-labeled variants of Aβ(1−16) were used. Two histidine residues at a time are isotopically labeled with ^{15}N. Upon ^{15}N substitution, the modulation depths of the frequencies due to ESEEM active ^{14}N nuclei will decrease. This decrease is because the single quantum transition of ^{15}N nuclei does not substantially contribute to the ESEEM signal.[64−69] We compare the integrated intensities of nonlabeled and ^{15}N-labeled variants. As the modulation depth of ^{1}H frequency is not affected by the ^{15}N substitution, the ^{1}H ESEEM peak is used to normalize the integrated intensity of ^{14}N ESEEM. Because two of the three histidine residues are labeled, the ^{14}N ESEEM signal intensity results only from the single nonlabeled histidine. This provides a direct method to determine the extent to which each histidine residue is involved in component II. All the samples were at pH 8.7, and the experiments were carried out at 3355 G, which corresponded to the maximum signal in the echo detected field sweep. The ESEEM intensities are integrated between 0 and 11 MHz in all the ESEEM spectra collected (Figure 7). The integrated ESEEM intensity of the His 6,13-labeled variant was ∼40% of that of the nonlabeled variant. In the His 6,13 variant, His 14 is the only labeled histidine residue and the ^{14}N ESEEM intensity results from only His 14. Likewise, His 13 contributes ∼40% and His 6, 20%, toward the component II Cu(II) coordination (Table 2).

Table 2. Contributions from Each Histidine Residue at Different pH Values of Cu(II)−Aβ(1−16) Complexes

pH	His 6	His 13	His 14
6.0 (comp I only)	50%	25%	25%
7.4 (comp I and II)	33%	33%	33%
8.7 (comp II only)	20%	40%	40%

The integrated intensities are tabulated in the Supporting Infomation (Table S2). To further confirm the proportions of the histidine residues, we performed the experiments using single-labeled variants in which only one histidine is labeled at a time. The decrease in the signal intensity in the ^{14}N ESEEM region with respect to the nonlabeled variant indicates the extent of the involvement of the labeled histidine in the coordination. The ESEEM spectra for single-labeled variants are shown in Figure S4, Supporting Infomation. The integrated ^{14}N ESEEM intensities (Table S3, Supporting Infomation) for single-label variants show the similar pattern of His 14 ≈ His 13 > His 6 as observed with the double-label variants.

This trend can be rationalized by the pK_a values of the histidine side chains. His 6 has a pK_a of 7.1, while for His 13 and 14 the pK_a values are 7.7 and 7.8, respectively.[70] As the imidazole ring in His 6 has a lower pK_a value, ring nitrogens will be deprotonated at lower pH values than in His 13 and 14. This deprotonation makes the ring nitrogens accessible for Cu(II) coordination. When the pH is raised, His 13 and 14 rings become more accessible for Cu(II) coordination. Hence the proportions of His 13 and 14 are increased with the increase in pH. These results are in accordance with an X-ray examination of Aβ(1−16), which suggests that His 13 and His 14 are readily accessible for metal ion coordination.[71] The design of a curcumin scaffold was discussed in this work, which is used to compete for Cu(II) coordination with the His 13−His 14 dyad.[71]

Hence, we suggest only one histidine residue is involved in component II, with a preference to His 13 and His 14 over His 6. The other residues involved in the component II coordination are the carbonyl oxygen of Ala 2,[72] the N-terminus (Asp 1),[43] and the amide nitrogen of Ala 2.[43] The peak around 2.8 MHz in the ESEEM spectra is indicative of backbone coordination and further confirms the involvement of the peptide backbone in component II coordination.[17,57,62,63] The possible subcomponents of component II are shown in Figure 8.

Our ESEEM results performed using both the double and single ^{15}N-labeled histidine residues indicate that His 13 and His 14 have a higher preference for the equatorial coordination position in Cu(II) component II coordination. Chemically, component II Cu(II) coordination is really interesting as Zn(II) is not able to displace Cu(II).[39] Biologically, it is important to understand the component II coordination, as component II may be the most significant Cu(II) coordination in vivo, as Zn(II) coexists with Cu(II). The insight into the component II coordination, more importantly the proportions of subcomponents, will shed light on understanding the role of metal ions in Alzheimer's disease.

■ CONCLUSIONS

We experimentally validated the use of ESEEM intensities to quantify the number of ^{14}N nuclei coupled to a Cu(II) ion. A monotonic increase in the ^{14}N ESEEM intensities were observed for the model complexes synthesized with different numbers of imidazole rings. Then, the validity of the method was tested with two well-characterized Cu(II) binding peptides. We used our method to solve an important structural problem in Aβ−Cu(II) complex. We determined that only a single histidine residue is coordinated to Cu(II) ion in component II in Aβ. Finally, in component II, Cu(II) uses His 13 and His 14 as an equatorial ligand over His 6. The proportions of the three histidine residues in Cu(II) coordination can be rationalized by the pK_a values of the histidine side chains. Shedding light into the component II coordination was critical as component II might be the dominant Cu(II) coordination mode of Aβ in vivo.

dx.doi.org/10.1021/jp500767n | J. Phys. Chem. B 2014, 118, 8935−8944

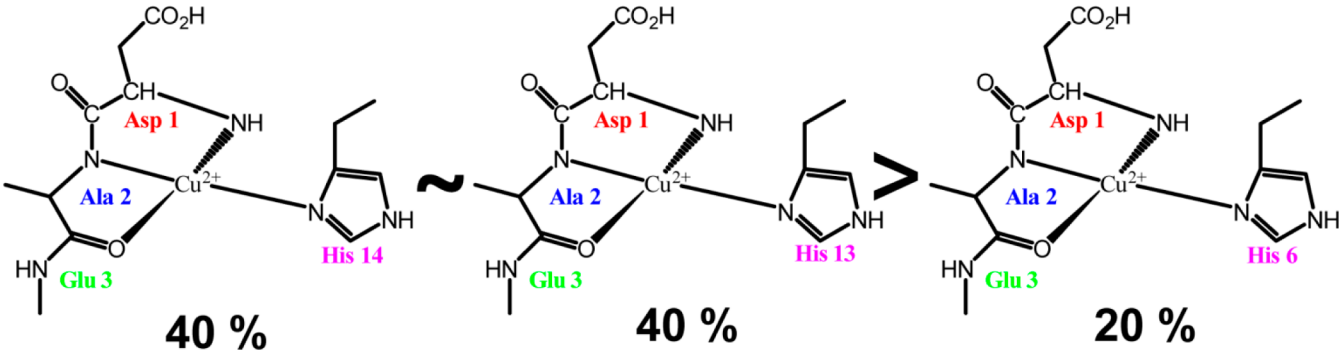

Figure 8. Different Cu(II) binding modes for component II. His 13 and His 14 equatorially coordinate to Cu(II) more than does His 6.

■ ASSOCIATED CONTENT

Supporting Information

CW simulations for model complexes (Figure S1), ESEEM simulation of model complexes (Figure S2), ESR parameters for ESEEM simulations (Table S1), error calculation method (Figure S3), single ^{15}N-labeled Aβ ESEEM spectra (Figure S4), and intensities of the ^{14}N-ESEEM and the ^{1}H-ESEEM region in the ESEEM spectra (Tables S2 and S3). This material is available free of charge via the Internet at http://pubs.acs.org.

■ AUTHOR INFORMATION

Corresponding Author

*(S.S.) E-mail: sksaxena@pitt.edu. Phone: (412) 624-8680. Fax: (412) 624-8611.

Notes

The authors declare no competing financial interest.

■ ACKNOWLEDGMENTS

We are grateful to the peptide synthesis facility at the University of Pittsburgh for peptide preparation. This work was supported by a National Science Foundation (MCB 1157712) grant. The Bruker ElexSys E680 FT/CW spectrometer was purchased with funds from National Institutes of Health Grant 1S10RR028701.

■ REFERENCES

(1) Malmström, B. G.; Leckner, J. The Chemical Biology of Copper. *Curr. Opin. Chem. Biol.* **1998**, *2*, 286−292.

(2) Deschampsa, P.; Kulkarnia, P. P.; Gautam-Basakb, M.; Sarkar, B. The Saga of Copper(II)−L-Histidine. *Coord. Chem. Rev.* **2005**, *249*, 895−909.

(3) Viles, J. H. Metal Ions and Amyloid Fiber Formation in Neurodegenerative Diseases. Copper, Zinc and Iron in Alzheimer's, Parkinson's and Prion Diseases. *Coord. Chem. Rev.* **2012**, *256*, 2271−2284.

(4) Faller, P.; Hureau, C. Bioinorganic Chemistry of Copper and Zinc Ions Coordinated to Amyloid-β Peptide. *Dalton Trans.* **2009**, 1080−1094.

(5) Binolfi, A. S.; Lamberto, G. R.; Duran, R.; Quintanar, L.; Bertoncini, C. W.; Souza, J. M.; Cerveñansky, C.; Zweckstetter, M.; Griesinger, C.; Fernández, C. O. Site-Specific Interactions of Cu(II) with α and β-Synuclein: Bridging the Molecular Gap between Metal Binding and Aggregation. *J. Am. Chem. Soc.* **2008**, *130*, 11801−11812.

(6) Binolfi, A.; Rodriguez, E. E.; Valensin, D.; D'Amelio, N.; Ippoliti, E.; Obal, G.; Duran, R.; Magistrato, A.; Pritsch, O.; Zweckstetter, M.; et al. Bioinorganic Chemistry of Parkinson's Disease: Structural Determinants for the Copper-Mediated Amyloid Formation of Alpha-Synuclein. *Inorg. Chem.* **2010**, *49*, 10668−10679.

(7) Drew, S. C.; Leong, S. L.; Pham, C. L. L.; Tew, D. J.; Masters, C. L.; Miles, L. A.; Cappai, R.; Barnham, K. J. Cu^{2+} Binding Modes of Recombinant α-Synuclein: Insights from EPR Spectroscopy. *J. Am. Chem. Soc.* **2008**, *130*, 7766−7773.

(8) Bortolus, M.; Bisaglia, M.; Zoleo, A.; Fittipaldi, M.; Benfatto, M.; Bubacco, L.; Maniero, A. L. Structural Characterization of a High Affinity Mononuclear Site in the Copper(II)−α-Synuclein Complex. *J. Am. Chem. Soc.* **2010**, *132*, 18057−18066.

(9) Dudzik, C. G.; Walter, E. D.; Millhauser, G. L. Coordination Features and Affinity of the Cu^{2+} Site in the α-Synuclein Protein of Parkinson's Disease. *Biochemistry* **2011**, *50*, 1771−1777.

(10) Binolfia, A.; Quintanarb, L.; Bertoncinic, C. W.; Griesingerd, C.; Fernández, C. O. Bioinorganic Chemistry of Copper Coordination to Alpha-Synuclein: Relevance to Parkinson's Disease. *Coord. Chem. Rev.* **2012**, *256*, 2188−2201.

(11) Rasia, R. M.; Bertoncini, C. W.; Marsh, D.; Hoyer, W.; Cherny, D.; Zweckstetter, M.; Griesinger, C.; Jovin, T. M.; Fernández, C. O. Structural Characterization of Copper(II) Binding to α-Synuclein: Insights into the Bioinorganic Chemistry of Parkinson's Disease. *Proc. Natl. Acad. Sci.* **2005**, *102*, 4294−4299.

(12) Aronoff-Spencer, E.; Burns, C. S.; Avdievich, N. I.; Gerfen, G. J.; Peisach, J.; Antholine, W. E.; Ball, H. L.; Cohen, F. E.; Prusiner, S. B.; Millhauser, G. L. Identification of the Cu^{2+} Binding Sites in the N-Terminal Domain of the Prion Protein by Epr and Cd Spectroscopy. *Biochemistry* **2000**, *39*, 13760−13771.

(13) Burns, C. S.; Aronoff-Spencer, E.; Legname, G.; Prusiner, S. B.; Antholine, W. E.; Gerfen, G. J.; Peisach, J.; Millhauser, G. L. Copper Coordination in the Full-Length, Recombinant Prion Protein. *Biochemistry* **2003**, *42*, 6794−6803.

(14) Klewpatinond, M.; Davie, P.; Bowen, S.; Brown, D. R.; Viles, J. H. Deconvoluting the Cu^{2+} Binding Modes of Full-Length Prion Protein. *J. Biol. Chem.* **2007**, *283*, 1870−1881.

(15) Millhauser, G. L. Copper and the Prion Protein: Methods, Structures, Function,and Disease. *Annu. Rev. Phys. Chem.* **2007**, *58*, 299−320.

(16) Walter, E. D.; Stevens, D. J.; Visconte, M. P.; Millhauser, G. L. The Prion Protein Is a Combined Zinc and Copper Binding Protein: Zn^{2+} Alters the Distribution of Cu^{2+} Coordination Modes. *J. Am. Chem. Soc.* **2007**, *129*, 15440−15441.

(17) Chattopadhyay, M.; Walter, E. D.; Newell, D. J.; Jackson, P. J.; Aronoff-Spencer, E.; Peisach, J.; Gerfen, G. J.; Bennett, B.; Antholine, W. E.; Millhauser, G. L. The Octarepeat Domain of the Prion Protein Binds Cu(II) with Three Distinct Coordination Modes at pH 7.4. *J. Am. Chem. Soc.* **2005**, *127*, 12647−12656.

(18) Jackson, G. S.; Murray, I.; Hosszu, L. L. P.; Gibbs, N.; Waltho, J. P.; Clarke, A. R.; Collinge, J. Location and Properties of Metal-Binding Sites on the Human Prion Protein. *Proc. Natl. Acad. Sci. U.S.A.* **2001**, *98*, 8531−8535.

(19) Jones, C. E.; Klewpatinond, M.; Abdelraheim, S. R.; Brown, D. R.; Viles, J. H. Probing Cu^{2+} Binding to the Prion Protein Using Diamagnetic Ni^{2+} and 1H NMR: The Unstructured N Terminus Facilitates the Coordination of Six Cu^{2+} Ions at Physiological Concentrations. *J. Mol. Biol.* **2005**, *346*, 1393−1407.

(20) Stellato, F.; Spevacek, A.; Proux, O.; Minicozzi, V.; Millhauser, G.; Morante, S. Zinc Modulates Copper Coordination Mode in Prion

Protein Octa-Repeat Subdomains. *Eur. Biophys J.* **2011**, *40*, 1259−1270.
(21) Morante, S.; González-Iglesias, R.; Potrich, C.; Meneghini, C.; Meyer-Klaucke, W.; Menestrina, G.; Gasset, M. Inter- and Intra-Octarepeat Cu(II) Site Geometries in the Prion Protein Implications in Cu(II) Binding Cooperativity and Cu(II)-Mediated Assemblies. *J. Biol. Chem.* **2004**, *279*, 11753−11759.
(22) Furlan, S.; Penna, G. L.; Guerrieri, F.; Morante, S.; Rossi, G. C. Ab Initio Simulations of Cu Binding Sites on the N-Terminal Region of Prion Protein. *J. Biol. Inorg. Chem.* **2007**, *12*, 571−583.
(23) Guerrieri, F.; Minicozzi, V.; Morante, S.; Rossi, G.; Furlan, S.; Penna, G. L. Modeling the Interplay of Glycine Protonation and Multiple Histidine Binding of Copper in the Prion Protein Octarepeat Subdomains. *J. Biol. Inorg. Chem.* **2009**, *14*, 361−374.
(24) Quintanar, L.; Rivillas-Acevedo, L.; Grande-Aztatzi, R.; Gómez-Castro, C. Z.; Arcos-López, T.; Vela, A. Copper Coordination to the Prion Protein: Insights from Theoretical Studies. *Coord. Chem. Rev.* **2013**, *257*, 429−444.
(25) Syme, C. D.; Nadal, R. C.; Rigby, S. E.; Viles, J. H. Copper Binding to the Amyloid-β (Aβ) Peptide Associated with Alzheimer's Disease: Folding, Coordination Geometry, pH Dependence, Stoichiometry, and Affinity of Aβ-(1−28): Insights from a Range of Complementary Spectroscopic Techniques. *J. Biol. Chem.* **2004**, *279*, 18169−18177.
(26) Guilloreau, L.; Damian, L.; Coppel, Y.; Mazarguil, H.; Winterhalter, M.; Faller, P. Structural and Thermodynamical Properties of Cuii Amyloid-β16/28 Complexes Associated with Alzheimer's Disease. *J. Biol. Inorg. Chem.* **2006**, *11*, 1024−1038.
(27) Shin, B.-K.; Saxena, S. Direct Evidence That All Three Histidine Residues Coordinate to Cu(II) in Amyloid-β(1−16). *Biochemistry* **2008**, *47*, 9117−9123.
(28) Morante, S. The Role of Metals in β-Amyloid Peptide Aggregation: X-Ray Spectroscopy and Numerical Simulations. *Curr. Alzheimer's Res.* **2008**, *5*, 508−524.
(29) Faller, P.; Hureau, C. Impact of Metallic Ions in Alzheimer's Disease: Insights from XAS Spectroscopy. *Actual. Chim.* **2011**, 356−357.
(30) Youssef, E. K.; Pierre, D.; Peter, F.; Petra, H. New Insights into the Coordination of Cu(II) by the Amyloid-β 16 Peptide from Fourier Transform Ir Spectroscopy and Isotopic Labeling. *J. Phys. Chem. B* **2011**, *115*, 14812−14821.
(31) Hureau, C.; Coppel, Y.; Dorlet, P.; Solari, P. L.; Sayen, S.; Guillon, E.; Sabater, L.; Faller, P. Deprotonation of the Asp1−Ala2 Peptide Bond Induces Modification of the Dynamic Copper(II) Environment in the Amyloid-β Peptide near Physiological pH. *Angew. Chem., Int. Ed.* **2009**, *48*, 9522−9525.
(32) Kowalik-Jankowska, T.; Ruta, M.; Wisniewska, K.; Łankiewicz, L. Coordination Abilities of the 1−16 and 1−28 Fragments of B-Amyloid Peptide Towards Copper(II) Ions: A Combined Potentiometric and Spectroscopic Study. *J. Inorg. Biochem.* **2003**, *95*, 270−282.
(33) Lu, Y.; Prudent, M.; Qiao, L.; Mendeza, M. A.; Girault, H. H. Copper(I) and Copper(II) Binding to β-Amyloid 16 (Aβ16) Studied by Electrospray Ionization Mass Spectrometry. *Metallomics* **2010**, *2*, 474−479.
(34) Raffa, D. F.; Gómez-Balderas, R.; Brunelle, P.; Rickard, G. A.; Rauk, A. Ab Initio Model Studies of Copper Binding to Peptides Containing a His−His Sequence: Relevance to the β-Amyloid Peptide of Alzheimer's Disease. *J. Biol. Inorg. Chem.* **2005**, *10*, 887−902.
(35) Rauk, A. Why Is the Amyloid Beta Peptide of Alzheimer's Disease Neurotoxic? *Dalton Trans.* **2008**, 1273−1282.
(36) Drew, S. C.; Noble, C. J.; Masters, C. L.; Hanson, G. R.; Barnham, K. J. Pleomorphic Copper Coordination by Alzheimer's Disease Amyloid-β Peptide. *J. Am. Chem. Soc.* **2009**, *131*, 1195−1207.
(37) Dorlet, P.; Gambarelli, S.; Faller, P.; Hureau, C. Pulse EPR Spectroscopy Reveals the Coordination Sphere of Copper(II) Ions in the 1−16 Amyloid-β Peptide: A Key Role of the First Two N-Terminus Residues. *Angew. Chem., Int. Ed.* **2009**, *48*, 9273−9276.
(38) Shin, B.-K.; Saxena, S. Substantial Contribution of the Two Imidazole Rings of the His13−His14 Dyad to Cu(II) Binding in Amyloid-β(1−16) at Physiological pH and Its Significance. *J. Phys. Chem. A* **2011**, *115*, 9590−9602.
(39) Silva, K. I.; Saxena, S. Zn(II) Ions Substantially Perturb Cu(II) Ion Coordination in Amyloid-β at Physiological pH. *J. Phys. Chem. B* **2013**, *117*, 9386−9394.
(40) Drew, S. C.; Noble, C. J.; Masters, C. L.; Hanson, G. R.; Barnham, K. J. Pleomorphic Copper Coordination by Alzheimer's Disease Amyloid-β Peptide. *J. Am. Chem. Soc.* **2009**, *131*, 1195−1207.
(41) Gunderson, W. A.; Hernández-Guzmán, J.; Karr, J. W.; Sun, L.; Szalai, V. A.; Warncke, K. Local Structure and Global Patterning of Cu^{2+} Binding in Fibrillar Amyloid-β [Aβ(1−40)] Protein. *J. Am. Chem. Soc.* **2012**, *134*, 18330−18337.
(42) Hureau, C. Coordination of Redox Active Metal Ions to the Amyloid Precursor Protein and to Amyloid-β Peptides Involved in Alzheimer Disease. Part 1: An Overview. *Coord. Chem. Rev.* **2012**, *256*, 2164−2174.
(43) Dorlet, P.; Gambarelli, S.; Faller, P.; Hureau, C. Pulse EPR Spectroscopy Reveals the Coordination Sphere of Copper(II) Ions in the 1−16 Amyloid-β Peptide: A Key Role of the First Two N-Terminus Residues. *Angew. Chem., Int. Ed.* **2009**, *48*, 9273−9276.
(44) Jun, S.; Gillespie, J. R.; Shin, B. K.; Saxena, S. The Second Cu(II)-Binding Site in a Proton-Rich Environment Interferes with the Aggregation of Amyloid-Beta(1−40) into Amyloid Fibrils. *Biochemistry* **2009**, *48*, 10724−10732.
(45) Alies, B.; Sasaki, I.; Sayen, S.; Guillon, E.; Faller, P.; Hureau, C. Zn Impacts Cu Coordination to Amyloid-β, the Alzheimer's Peptide, but Not the Ros Production and the Associated Cell Toxicity. *Chem. Commun.* **2013**, *49*, 2130−2132.
(46) Lovell, M. A.; Robertsona, J. D.; Teesdaleb, W. J.; Campbell, J. L.; Markesbery, W. R. Copper, Iron and Zinc in Alzheimer's Disease Senile Plaques. *J. Neurol. Sci.* **1998**, *158*, 47−52.
(47) McCracken, J.; Desai, P. R.; Papadopoulos, N. J.; Villafranca, J. J.; Peisach, J. Electron Spin-Echo Studies of the Copper(II) Binding Sites in Dopamine β-Hydroxylase. *Biochemistry* **1988**, *27*, 4133−4137.
(48) Goldfarb, D.; Fauth, J.-M.; Tor, Y.; Shanzer, A. Study of Cu(II) Binding to Chiral Tripodal Ligands by Electron Spin Echo Spectroscopy. *J. Am. Chem. Soc.* **1991**, *113*, 1941−1948.
(49) Fransson, G.; Lundberg, B. K. S. Metal Complexes with Mixed Ligands, 4. The Crystal Structure of Tetrakisimidazole Cu(II) Sulphate, $Cu(C_3H_4N_2)_4so_4$. *Acta Chem. Scand.* **1972**, *26*, 3969−3976.
(50) Abuhijleh, A. L.; Woods, C.; Ahmed, I. Y. Synthesis and Molecular Structure of Monomeric Copper(II) Acetates with 2-Methylimidazole and 1,2-Dimethylimidazole. *Inorg. Chim. Acta* **1990**, *190*, 11−17.
(51) Sato, M.; Nagae, S.; Ohmae, K.; Nakaya, J.-I. Preparation and Crystal Structure of an Imidazolate: Bridged Polynuclear Complex [{Cu(Im)(Dien)}N][ClO4]N (Dien = Diethylenetriamine), and Its Properties in Dimethyl Sulfoxide Solution. *J. Chem. Soc., Dalton Trans.* **1986**, 1949.
(52) Merrifield, R. B. Solid Phase Peptide Synthesis. I. The Synthesis of a Tetrapeptide. *J. Am. Chem. Soc.* **1963**, *85*, 2149−2154.
(53) Fields, G. B.; Noble, R. L. Solid Phase Peptide Synthesis Utilizing 9-Fluorenylmethoxycarbonyl Amino Acids. *Int. J. Pept. Protein Res.* **1990**, *35*, 161−214.
(54) Fauth, J. M.; Schweiger, A.; Braunschweiler, L.; Forrer, J.; Ernst, R. R. Elimination of Unwanted Echoes and Reduction of Deadtime in Three-Pulse Electron Spin-Echo Spectroscopy. *J. Magn. Reson.* **1986**, *66*, 74.
(55) Gemperle, C.; Aebli, G.; Schweiger, A.; Ernst, R. R. Phase Cycling in Pulse EPR. *J. Magn. Reson.* **1990**, *88*, 241.
(56) Guilloreau, L.; Combalbert, S.; Sournia-Saquet, A.; Mazarguil, H.; Faller, P. Redox Chemistry of Copper−Amyloid-β: Thegeneration of Hydroxyl Radical in the Presenceof Ascorbate Is Linked to Redox-Potentials and Aggregation State. *ChemBioChem* **2007**, *8*, 1317−1325.
(57) Burns, C. S.; Aronoff-Spencer, E.; Dunham, C. M.; Lario, P.; Avdiech, N. I.; Antholine, W. E.; Olmstead, M. M.; Vrielink, A.; Gerfen, G. J.; Peisach, J.; et al. Molecular Features of the Copper Binding Sites in the Octarepeat Domain of the Prion Protein. *Biochemistry* **2002**, *41*, 3991−4001.

(58) Deligiannakis, Y.; Louloudib, M.; Hadjiliadis, N. Electron Spin Echo Envelope Modulation (ESEEM) Spectroscopy as a Tool to Investigate the Coordination Environment of Metal Centers. *Coord. Chem. Rev.* **2000**, *201*, 1−112.
(59) Peisach, J.; Blumberg, W. E. Structural Implications Derived from the Analysis of EPR Spectra of Natural and Artificial Copper Proteins. *Arch. Biochem. Biophys.* **1974**, *165*, 691−708.
(60) Hernández-Guzmán, J.; Sun, L.; Mehta, A. K.; Dong, J.; Lynn, D. G.; Warncke, K. Copper(II)-Bis-Histidine Coordination Structure in a Fibrillar Amyloid β-Peptide Fragment and Model Complexes Revealed by Electron Spin Echo Envelope Modulation Spectroscopy. *ChemBioChem* **2013**, *14*, 1762−1771.
(61) McCracken, J.; Pember, S.; Benkovic, S. J.; Villafranca, J. J.; Miller, R. J.; Peisach, J. Electron Spin-Echo Studies of the Copper Binding Site in Phenylalanine Hydroxylase from Chromobacterium Violaceum. *J. Am. Chem. Soc.* **1988**, *110*, 1069−1074.
(62) Burns, C. S.; Aronoff-Spencer, E.; Dunham, C. M.; Lario, P.; Avdievich, N. I.; Antholine, W. E.; Olmstead, M. M.; Vrielink, A.; Gerfen, G. J.; Peisach.; et al. Molecular Features of the Copper Binding Sites in the Octarepeat Domain of the Prion Protein. *Biochemistry* **2002**, *41*, 3991−4001.
(63) Shin, B.-K.; Saxena, S. Insight into Potential Cu(II)-Binding Motifs in the Four Pseudorepeats of Tau Protein. *J. Phys. Chem. B* **2011**, *115*, 15067−15078.
(64) McCracken, J.; Peisach, J.; Cote, C. E.; McGuirl, M. A.; Dooley, D. M. Pulsed EPR Studies of the Semiquinone State of Copper-Containing Amine Oxidases. *J. Am. Chem. Soc.* **1992**, *114*, 3715−3720.
(65) Mims, W. B. Envelope Modulation in Spin-Echo Experiments. *Phys. Rev. B* **1972**, *5*, 2409−2419.
(66) Lai, A.; Flanagan, H. L.; Singel, D. J. Multifrequency Electron Spin Echo Envelope Modulation in S = 1/2, I = 1/2 Systems: Analysis of the Spectral Amplitudes, Line Shapes, and Linewidths. *J. Chem. Phys.* **1988**, *89*, 7161−7166.
(67) Tang, X. S.; Diner, B. A.; Larsen, B. S.; Gilchrist, M. L., Jr.; Lorigan, G. A.; Britt, R. D. Identification of Histidine at the Catalytic Site of the Photosynthetic Oxygen-Evolving Complex. *Proc. Natl. Acad. Sci. U.S.A.* **1994**, *91*, 704−708.
(68) Singh, V.; Zhu, Z.; Davidson, V. L.; McCracken, J. Characterization of the Tryptophan Tryptophyl-Semiquinone Catalytic Intermediate of Methylamine Dehydrogenase by Electron Spin-Echo Envelope Modulation Spectroscopy. *J. Am. Chem. Soc.* **2000**, *122*, 931−938.
(69) Stoll, S.; Calle, C.; Mitrikas, G.; Schweiger, A. Peak Suppression in Eseem Spectra of Multinuclear Spin Systems. *J. Magn. Reson.* **2005**, *177*, 93−101.
(70) Ma, K.; Clancy, E. L.; Zhang, Y.; Ray, D. G.; Wollenberg, K.; Zagorski, M. G. Residue-Specific pK_a Measurements of the β-Peptide and Mechanism of pH-Induced Amyloid Formation. *J. Am. Chem. Soc.* **1999**, *121*, 8698−8706.
(71) Zhang, X.; Tian, Y.; Li, Z.; Tian, X.; Sun, H.; Liu, H.; Moore, A.; Ran, C. Design and Synthesis of Curcumin Analogues for in Vivo Fluorescence Imaging and Inhibiting Copper-Induced Cross-Linking of Amyloid Beta Species in Alzheimer's Disease. *J. Am. Chem. Soc.* **2013**, *135*, 16397−16409.
(72) Drew, S. C.; Masters, C. L.; Barnham, K. J. Alanine-2 Carbonyl Is an Oxygen Ligand in Cu^{2+} Coordination of Alzheimer's Disease Amyloid-B Peptide: Relevance to N-Terminally Truncated Forms. *J. Am. Chem. Soc.* **2009**, *131*, 8760−8761.